Macromolecules

Article

pubs.acs.org/Macromolecules

Computer Simulations of Bottle Brushes: From Melts to Soft Networks

Zhen Cao,[†] Jan-Michael Y. Carrillo,[‡,§] Sergei S. Sheiko,[∥] and Andrey V. Dobrynin*[,†]

[†]Polymer Program and Institute of Materials Science, University of Connecticut, Storrs, Connecticut 06269-3136, United States

[‡]Center for Nanophase Materials Sciences and [§]Computer Science and Mathematics Division, Oak Ridge National Laboratory, Oak Ridge, Tennessee 37831, United States

[∥]Department of Chemistry, University of North Carolina, Chapel Hill, North Carolina 27599-3220, United States

ABSTRACT: Using a combination of molecular dynamics simulations and analytical calculations, we study dense bottle-brush systems in a melt and network state. Analysis of our simulation results shows that bottle-brush macromolecules in melt behave as ideal chains with effective Kuhn length b_K. Simulations show that the bottle-brush-induced bending rigidity is due to an entropy decrease caused by redistribution of the side chains upon backbone bending. The Kuhn length of the bottle brushes increases with increasing the side-chain degree of polymerization n_{sc} as $b_K \propto n_{sc}^{0.46}$. This model of bottle-brush macromolecules is extended to describe mechanical properties of bottle-brush networks in linear and nonlinear deformation regimes. In the linear deformation regime, the network shear modulus scales with the degree of polymerization of the side chains as $G_0 \propto (n_{sc} + 1)^{-1}$ as long as the ratio of the Kuhn length, b_K, to the size of the fully extended bottle-brush backbone between cross-links, R_{max}, is smaller than unity, $b_K/R_{max} \ll 1$. Bottle-brush networks with $b_K/R_{max} \propto 1$ demonstrate behavior similar to that of networks of semiflexible chains with $G_0 \propto n_{sc}^{-0.5}$. In the nonlinear network deformation regime, the deformation-dependent shear modulus is a universal function of the first strain invariant I_1 and bottle-brush backbone deformation ratio β describing stretching ability of the bottle-brush backbone between cross-links.

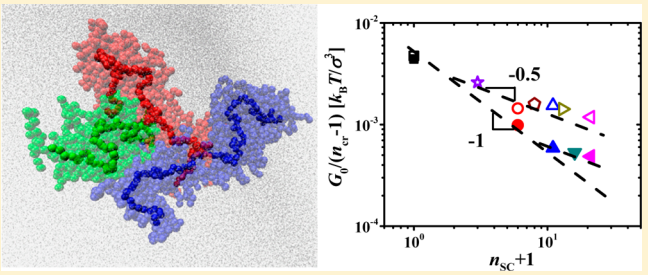

INTRODUCTION

Elasticity of polymeric networks originates from deformation of the individual polymer strands making up the network.[1,2] Under applied external stress these strands extend reducing the number of available conformations and therefore decreasing the total entropy of the system. The network shear modulus G is proportional to product of number density of polymeric strands ρ_{ch} and thermal energy k_BT (where k_B is the Boltzmann constant and T is the absolute temperature). In dry (solvent-free) networks, the strands number density ρ_{ch} is inversely proportional to the number-average degree of polymerization, N_s, of network strands, resulting in $G \propto N_s^{-1}$. This suggests that polymeric networks could be made softer by decreasing cross-linking density, i.e., increasing N_s. However, this scaling relation holds until the degree of polymerization of strands between cross-links, N_s, is below the degree of polymerization between entanglements of overlapping strands, N_e.[1,3] For longer network strands, $N_s > N_e$, these entanglements are locked by cross-linking reaction and thus restrict configurational space accessible to polymeric strands. As such, the entanglements play a role of topological cross-links that control elastic properties of the networks as modulus saturates at $G \sim 1/N_e$. For dry polymeric networks, this imposes a lower limit on the network shear modulus to be on the order of 0.1 MPa independent of the chemical degree of polymerization $N_s > N_e$.

These topological constraints (chain entanglements) pose challenges in making supersoft networks with shear modulus below 1000 Pa that could be good candidates for synthetic substitutes of biological tissues.[4−6] Note that these values of the shear modulus could be achieved in polymeric gels, but this requires for gel to be swollen in a solvent which may leak upon gel deformation and dry upon storage. There are several approaches that allow overcoming this restriction. In the first approach networks are prepared by cross-linking polymer chains in a semidilute solution followed by the solvent evaporation.[7,8] This results in remarkably stretchable elastomers with the ultimate strain over 3000%.[8] The second group of approaches utilizes synthetic modifications of polymer chains to increase effective entanglement molecular weight through chain branching in combs, stars, dendrimers, and bottle brushes.[9−19] This may be considered as effective dilution of a polymer network by binding solvent molecules to macromolecules. Bottle-brush systems (see Figure 1) are the most promising example of the modification of the macromolecular structures achieving the entanglement shear modulus G_e to be on the order of 100 Pa with increasing the degree of polymerization of the side chains.[17] In this paper, we use a

Received: April 1, 2015
Revised: June 24, 2015
Published: July 13, 2015

DOI: 10.1021/acs.macromol.5b00682
Macromolecules 2015, 48, 5006−5015

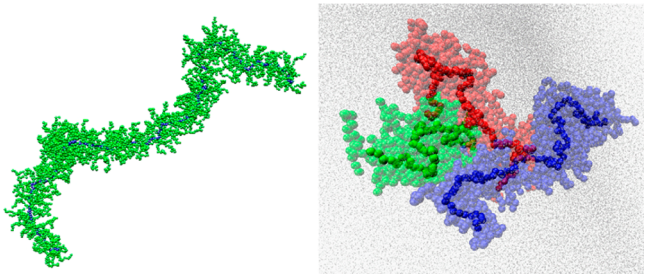

Figure 1. Bottle-brush macromolecule with N monomers belonging to bottle-brush backbone colored in blue and side chains consisting of n_{sc} monomers shown in green (left). Snapshot of the bottle-brush network with three individual bottle-brush macromolecules highlighted (right).

combination of molecular dynamics simulations and theoretical calculations to study elasticity of networks made by cross-linking bottle-brush macromolecules and show how to relate these properties to structure of bottle brushes in a melt.

RESULTS AND DISCUSSION

To study properties of the bottle-brush networks, we have performed coarse-grained molecular dynamics simulations[20] of cross-linked bottle-brush macromolecules. In our simulations polymer chains making up bottle-brush macromolecules were modeled by Lennard-Jones particles (beads) with diameter σ connected by the FENE bonds (see Figure 1). For all studied systems the number of monomers (beads) in the bottle-brush backbone was equal to $N = 100$ with every monomer of the backbone having a side chain attached to it. The number of monomers in the side chains, n_{sc}, was varied between 0 (linear chains) and 20. The networks were prepared by randomly cross-linking melt of bottle-brush chains at monomer concentration $0.8\sigma^{-3}$. Simulation details are described in Simulation Methods section.

Properties of Bottle-Brush Melt. We begin our discussion by presenting results of molecular dynamics simulations of melts of bottle-brush macromolecules. The purpose of this initial study is to understand factors controlling bending rigidity and, hence, the Kuhn length, b_K, of individual bottle-brush macromolecules in a melt. This will allow mapping bottle-brush macromolecules into the discrete chain model with internal bending rigidity[21] that was recently applied to describe nonlinear elasticity of polymeric and biological networks and gels.[22,23]

The Kuhn length of a bottle-brush macromolecule is obtained from bond−bond correlation function. This function describes decay of the orientational memory along the bottle-brush backbone between two unit bond vectors $\vec{n}_i$ and $\vec{n}_{i+l}$ pointing along the backbone bonds and separated by l-bonds as shown in the inset of Figure 2. This function is defined as

$$G(l) = \frac{1}{N_b - l} \sum_{i=1}^{N_b - l} \langle (\vec{n}_i \cdot \vec{n}_{i+l}) \rangle \qquad (1)$$

where $N_b = N - 1$ is the number of bonds in the bottle-brush backbone and the brackets $\langle\ \rangle$ denote averaging over backbone configurations. Figure 2 shows dependence of the backbone bond−bond correlation function on the side chain degree of polymerization, n_{sc}. As follows from this figure, bottle brushes become stiffer with increasing the degree of polymerization of the side chains. Furthermore, one can identify two different

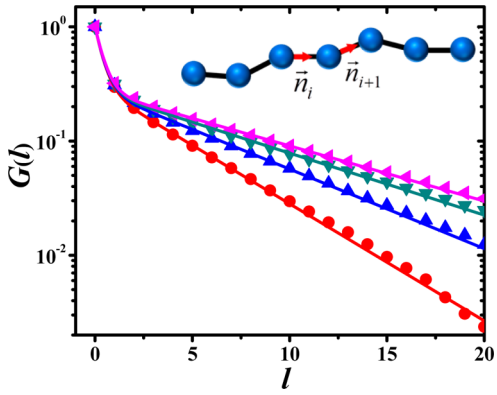

Figure 2. Bond−bond correlation function of the bottle-brush backbone in a melt of bottle-brush macromolecules with the degree of polymerization of the side chains $n_{sc} = 5$ (red circles), $n_{sc} = 10$ (blue triangles), $n_{sc} = 15$ (cyan inverted triangles), and $n_{sc} = 20$ (pink triangles). The solid lines correspond to the fitting results using double-exponential function given by eq 2. FENE potential spring constant $k_{spring} = 30k_BT/\sigma^2$ for all data sets. Inset shows schematic representation of the bottle-brush backbone with unit bond vectors.

regimes in the bond−bond correlation functions in Figure 2. All curves first show a fast drop of the orientational memory followed by a much slower memory decay with increasing number of bonds between unit bond vectors. This form of the bond−bond correlation function resembles that observed in polyelectrolytes, where electrostatic interactions between charged groups induce chain bending rigidity.[24−26] For polyelectrolytes, the existence of two regimes with fast and slow decay of the orientational memory is a manifestation of two different mechanisms of chain deformation. At short length scales, the bonds' orientational memory is due to local chain tension, while at the longer length scales, it is determined by chain's bending rigidity induced by long-range electrostatic interactions. Thus, we can argue that steric interactions between side chains in the bottle-brush macromolecules play a role similar to electrostatic interactions in polyelectrolyte systems, i.e., increasing bending rigidity of bottle-brush macromolecules. To test this hypothesis, we fit data sets shown in Figure 2 by empirical bond−bond correlation function in the following form:[24]

$$G(l) = (1 - \alpha) \exp\left(-\frac{|l|}{\lambda_1}\right) + \alpha \exp\left(-\frac{|l|}{\lambda_2}\right) \qquad (2)$$

where α, λ_1, and λ_2 are fitting parameters. Indeed, one can see a very good fit of the simulation data by sum of two exponential functions. It is important to point out that our approach to describe bottle-brush bending properties is different from a single-exponential fit used in refs 27−31 at short length scales. By utilizing a single-exponential function to fit simulation data at short length scales, one neglects local stretching of the backbone induced by interactions between the neighboring side chains and its contribution to the bottle-brush Kuhn length. Note that at the longer length scales, however, the bond−bond correlation function begins to deviate from the double-exponential form given by eq 2 and in accordance with ref 29 should follow power law decay. Unfortunately, for studied backbone degree of polymerization, we have not been able clearly identify this regime.

We can further verify the validity of the correlation function given by eq 2 to describe bottle-brush backbone bending

DOI: 10.1021/acs.macromol.5b00682
Macromolecules 2015, 48, 5006−5015

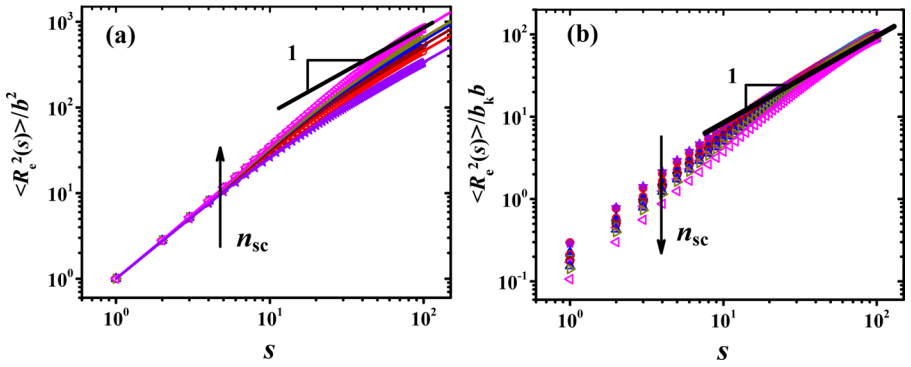

Figure 3. Dependence of the mean-square end-to-end distance of the section of the bottle-brush backbone in a melt. Plots of $\langle R_e^2(s)\rangle/b^2$ (a) and $\langle R_e^2(s)\rangle/bb_K$ (b) as a function of the number of bonds s in a section of the bottle-brush backbone for bottle-brush macromolecules with values of the FENE potential spring constants $k_{spring} = 500k_BT/\sigma^2$ (solid symbols) and $k_{spring} = 30k_BT/\sigma^2$ (open symbols) and degree of polymerization of the side chains: $n_{sc} = 2$ (violet stars), $n_{sc} = 5$ (red circles), $n_{sc} = 7$ (wine pentagons), $n_{sc} = 10$ (blue triangles), $n_{sc} = 12$ (yellow right triangles), $n_{sc} = 15$ (cyan inverted triangles), and $n_{sc} = 20$ (pink left triangles). The solid lines in (a) correspond to eq 4.

rigidity by comparing the analytically calculated mean-square end-to-end distance of a backbone section with s-bonds

$$\langle R_e^2(s)\rangle = \frac{1}{N_b - s}\sum_{i=1}^{N-s}\langle(\vec{r}_i - \vec{r}_{i+s})^2\rangle \tag{3}$$

using for bond−bond correlation function expression eq 2 and those obtained from simulations. In eq 3, $\vec{r}_i$ is the radius vector of the ith monomer on the bottle-brush backbone. For bond−bond correlation function given by eq 2, the mean-square end-to-end distance of the section of the chain can be written as follows

$$\langle R_e^2(s)\rangle = b^2((1-\alpha)g(\lambda_1, s) + \alpha g(\lambda_2, s)) \tag{4}$$

where b is the bond length and function

$$g(\lambda, s) = s\frac{1 + e^{-1/\lambda}}{1 - e^{-1/\lambda}} - 2e^{-1/\lambda}\frac{1 - e^{-s/\lambda}}{(1 - e^{-1/\lambda})^2} \tag{5}$$

Note that the calculations are similar to those used for calculation of the mean-square value of the end-to-end distance of a chain with a fixed bond angle as discussed elsewhere.[2,32] The data points in Figure 3a show our simulation data while the lines correspond to eq 4. This figure suggests that short backbone segments with $s < 10$ are not fully stretched since the scaling dependence of $\langle R_e^2(s)\rangle$ on s is weaker than quadratic. In addition, the stretching of the backbone at small length scales is independent of the degree of polymerization of the side chains and is controlled by local packing and interactions between monomers in the vicinity of grafting points. Note that for large backbone sections with the number of bonds s in a backbone segment approaching N_b, the mean-square end-to-end distance $\langle R_e^2(s)\rangle$ demonstrates linear scaling dependence. This is expected for an ideal chain with an effective Kuhn length, b_K. The b_K of the bottle-brush macromolecules can be obtained from eq 4 in the limit when both s/λ_1 and s/λ_2 are larger than unity

$$b_K = \left.\frac{\langle R_e^2(s)\rangle}{sb}\right|_{s\gg 1} \approx b((1-\alpha)h(\lambda_1) + \alpha h(\lambda_2)) \tag{6}$$

where we introduced function $h(\lambda)$

$$h(\lambda) = \frac{1 + e^{-1/\lambda}}{1 - e^{-1/\lambda}} \tag{7}$$

Figure 3b confirms that bottle-brush macromolecules at large length scales behave as ideal chains with Kuhn length b_K and bond length b. All our data sets in the range of large s can be collapsed into one universal curve by normalizing $\langle R_e^2(s)\rangle$ by the product $b_K b$.

Figure 4 shows how the bottle-brush Kuhn length (eq 6) depends on the number of monomers in the side chains for two

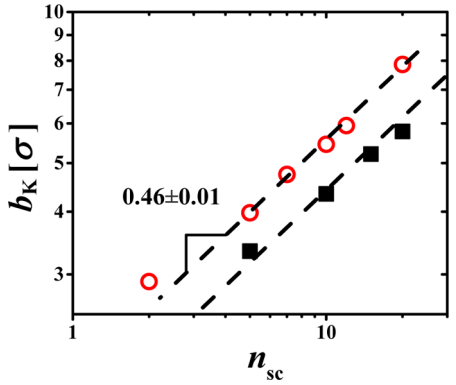

Figure 4. Dependence of the Kuhn length b_K on the side chain degree of polymerization n_{sc} for bottle-brush macromolecules with two different values of the FENE potential spring constants: $k_{spring} = 30k_BT/\sigma^2$ (filled squares) and $k_{spring} = 500k_BT/\sigma^2$ (open circles).

different spring constants of the FENE potential. As expected, the scaling dependence does not depend on the potential strength, while the stronger spring constant results in larger Kuhn length. This is ascribed to a shorter bond length b, resulting in stronger crowding of monomers close to the grafting points of the side chains to the bottle-brush backbone, which in turn stiffens the bottle brush. Note that both data sets show scaling exponent close to 0.5. The error estimate for scaling exponent was obtained by using jackknife method.[33] The data for the bottle-brush Kuhn length can also be presented as a function of the bottle-brush diameter, which provides information about the aspect ratio of the Kuhn segment. In Figure 5a, we plot dependence of the bottle-brush diameter D defined as

$$D^2 = 4\langle R_g^2\rangle = \frac{4}{n_{sc}^2}\sum_{i<j}^{n_{sc}}\langle(\vec{r}_i - \vec{r}_j)^2\rangle \tag{8}$$

DOI: 10.1021/acs.macromol.5b00682
Macromolecules 2015, 48, 5006−5015

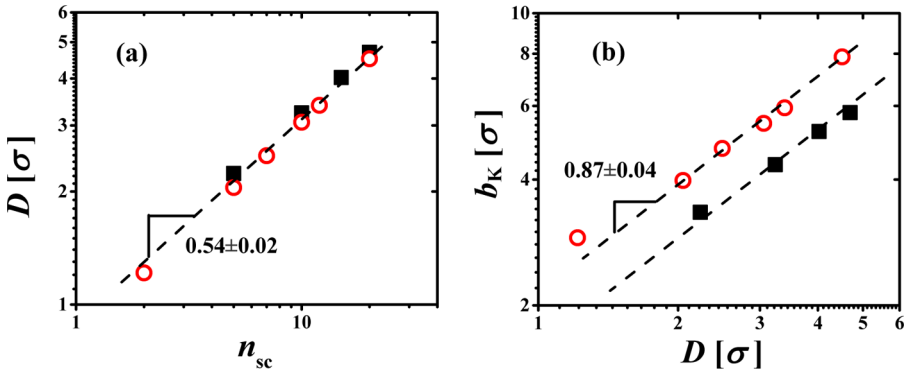

Figure 5. (a) Dependence of the bottle-brush diameter on the side chain degree of polymerization. (b) Dependence of the Kuhn length on the bottle-brush diameter. Notations are the same as in Figure 4.

on the degree of polymerization of the side chains, n_{sc}. Both data sets exhibit nearly the same scaling dependence $D \propto n_{sc}^{0.54}$, which indicates that in average the side chain conformations are close to that of an ideal chain. Figure 5b shows that the Kuhn length of the bottle brush is only slightly longer than diameter D, suggesting that bottle-brush macromolecules in a melt state can be presented as random walk of effective monomers of size equal to bottle-brush diameter similar to the case of single bottle-brush macromolecules.[31]

The slight extension of the side chains with respect to the ideal chain dimensions is ascribed to the crowded environment in the vicinity of the backbone, which leads to nonuniform stretching of the side chains. As shown in Figure 6, the

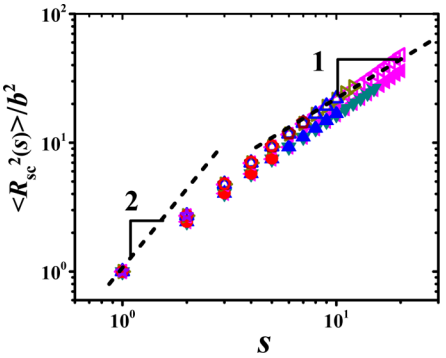

Figure 6. Mean-square end-to-end distance of the section of the bottle-brush side chain for bottle-brush macromolecules with two different values of the FENE potential spring constants: $k_{spring} = 30k_BT/\sigma^2$ (filled symbols) and $k_{spring} = 500k_BT/\sigma^2$ (open symbols) and degree of polymerization of the side chains: $n_{sc} = 2$ (violet stars), $n_{sc} = 5$ (red circles), $n_{sc} = 7$ (wine pentagons), $n_{sc} = 10$ (blue triangles), $n_{sc} = 12$ (army green right triangles), $n_{sc} = 15$ (cyan inverted triangles), and $n_{sc} = 20$ (pink left triangles).

elongation of the side chains is stronger close to the grafting points while it decreases toward the side chain end. However, even at the bottle-brush backbone, the chains are not fully stretched resulting in weaker than linear dependence of the section size $R_{sc}(s)$ on the number of bonds s. Note that we are measuring side chain size $R_{sc}(s)$ from the grafting point.

In order to elucidate the molecular mechanism of bottle-brush bending rigidity, we have calculated probability distribution functions of orientation of the end-to-end vectors of the side chains and their deformation in the local system of coordinates associated with the bending plane of the backbone. For each monomer on the backbone, we have defined the backbone bending plane by combining backbone bonds in groups of three for each monomer as shown in Figure 7. This

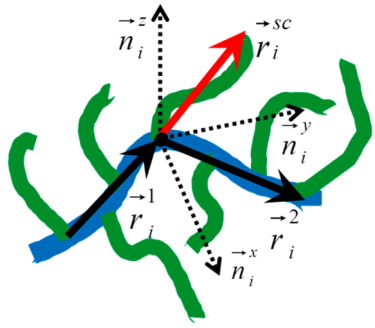

Figure 7. Schematic representation of the bottle-brush backbone sections and definition of the local system of coordinates.

procedure defines a set of unit vectors $\{\vec{n}_i^1, \vec{n}_i^2\}$ pointing along radius vectors $\vec{r}_i^1$ and $\vec{r}_i^2$. In order to minimize the end effects, we have excluded three side chains at each end of the backbone. Each pair of the vectors $\vec{n}_i^1$ and $\vec{n}_i^2$ determines the backbone bending plane, and their cross-product, $\vec{n}_i^z = \vec{n}_i^2 \times \vec{n}_i^1/|\vec{n}_i^2 \times \vec{n}_i^1|$, defines the direction normal to this plane. The unit vector pointing in the direction of the local backbone bending is defined as $\vec{n}_i^x = (\vec{n}_i^2 - \vec{n}_i^1)/|\vec{n}_i^2 - \vec{n}_i^1|$. To complete the local system of coordinates, we introduce a unit vector pointing along the y-axis $\vec{n}_i^y = \vec{n}_i^z \times \vec{n}_i^x/|\vec{n}_i^z \times \vec{n}_i^x|$.

Figures 8a–c show projections on the x–y plane of the orientational distribution functions of the unit vectors pointing along the end-to-end vectors of the side chains and side chain sections (see Figure 7). These figures clearly illustrate redistribution of the side chains between concave and convex regions of the bottle-brush backbone upon its bending. The redistribution is especially evident for shorter side chains (Figure 8a). For longer side chains this redistribution is less pronounced as shown in Figure 8b. However, in this case, the correlation between orientation of the side chain sections and the bending direction can be clearly seen for section of the side chains close to the bottle-brush backbone. Furthermore, redistribution of the side chains from the concave bottle-brush bending region decreases extension of the side chains as shown in Figures 8d–f. It is important to point out, however, that stretching of the chains in the concave bottle-brush bending region is relatively weak and is below 5% of the ideal size of the side chain except for sections of the side chains close to the bottle-brush backbone (see Figure 8f).

DOI: 10.1021/acs.macromol.5b00682
Macromolecules 2015, 48, 5006–5015

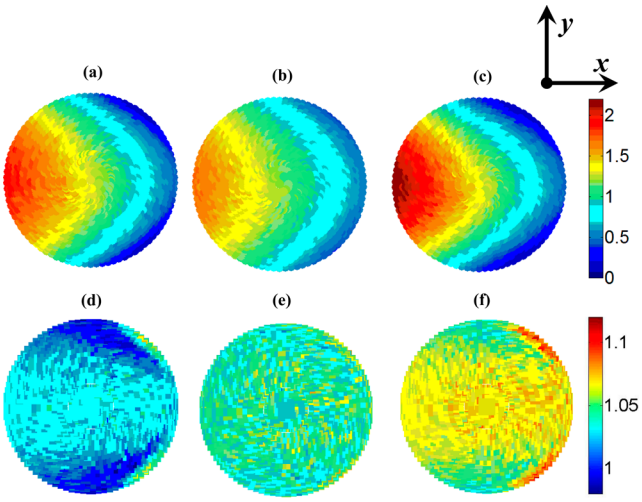

Figure 8. Projection on the $x-y$ plane of distribution function of the orientations of the unit vectors pointing in the direction of the end-to-end vectors of the side chains for bottle-brush macromolecules with n_{sc} = 5 (a) and n_{sc} = 20 (b) and for the section of the side chain containing the first five bonds of the bottle-brush chain with n_{sc} = 20 (c). Projection on the $x-y$ plane of the orientational distribution function of the deformation $(\langle R_{sc}^2\rangle/\langle R_0^2\rangle)^{1/2}$ of the side chains for bottle-brush macromolecules with n_{sc} = 5 (d) and n_{sc} = 20 (e) and for the section of the side chain containing the first five bonds of the bottle-brush chain with n_{sc} = 20 (f). The ideal chain size R_0 was obtained from simulations of linear chains in a melt. FENE potential spring constant $k_{spring} = 500k_BT/\sigma^2$ for all data sets.

We will assume that the side chain redistribution is a driving force behind bottle-brush bending rigidity and will use this mechanism to derive the effective bending constant of a bottle brush. In our approach we will map bottle-brush macromolecule into a chain with bending rigidity. According to this chain model, the Kuhn length b_K of the bottle-brush macromolecules with diameter D and bending constant K_D is equal to[21]

$$b_K \approx D\frac{1 + \coth(K_D) - K_D^{-1}}{1 - \coth(K_D) + K_D^{-1}} \tag{9}$$

In our calculations of the bottlebrush bending constant K_D, we will bend a cylinder with diameter D occupied by bottle brush into a toroidal sector with radius of curvature R (Figure 9). Consider deformation of the section of the cylinder with length D equal to the diameter into a toroidal sector with angle θ and having volume

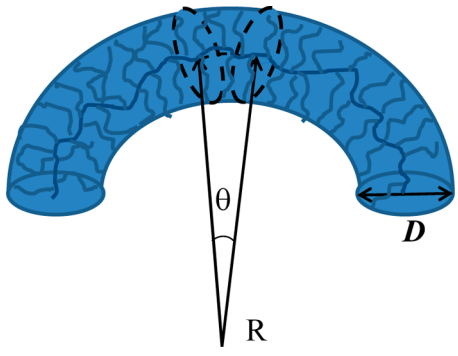

Figure 9. Schematic representation of bending of a bottle-brush macromolecule.

$$\delta V(\theta) \approx \frac{\pi}{4}\theta R D^2 \approx \frac{\pi}{4}D^3 \tag{10}$$

In order to maintain monomer density within the toroidal sector constant, the side chains should redistribute between upper and bottom parts of the sector. The number of the side chains in the upper, $m_u(\theta)$, and bottom, $m_b(\theta)$, parts of the toroidal sector is proportional to their volumes

$$m_u(\theta) \approx m_D\left(\frac{1}{2} + \frac{D}{3\pi R}\right) \quad \text{and} \quad m_b(\theta) \approx m_D\left(\frac{1}{2} - \frac{D}{3\pi R}\right) \tag{11}$$

where m_D is the number of the side chains within deformed volume $\delta V(\theta)$. Redistribution of the side chains due to cylinder bending results in change of the bottle-brush configurational free energy. This can be estimated as a change of the free energy due to partitioning of side chains into two groups with number of side chains in each group to be $m_u(\theta)$ and $m_b(\theta)$. For small bending angles θ this free energy change is

$$\frac{\Delta F_{bend}(\theta)}{k_BT} \approx \frac{2}{9\pi^2}m_D\theta^2 \tag{12}$$

The effective bending constant of the bottlebrush chain K_D is estimated by mapping deformation of the bottle brush on that of a chain with internal bending rigidity K_D and bond length D. For such chain the bending energy per bond due to bending on small-angle θ is equal to $K_D\theta^2/2$. Comparing this expression with eq 12, we obtain for bending constant of a bottle brush

$$K_D \approx \frac{4}{9\pi^2}m_D \approx \frac{4}{9\pi^2}\frac{D}{b} \tag{13}$$

where we assume that the bottle-brush backbone is almost fully stretched such that $m_D \approx D/b$. Analysis of eqs 13 and 9 and data shown in Figure 5a indicates that for our systems (D/b < 5) K_D < 1 and $b_K \approx D$, which is in agreement with the scaling coefficient 0.87 ± 0.04 in Figure 5b. The weaker than linear dependence results from the ratio 0.46/0.54 = 0.85 of the corresponding scaling exponents for b_K and D on degree of polymerization of the side chains n_{sc} shown in Figures 4 and 5a, respectively.

Note that our conclusion about flexible nature of the bottle-brush macromolecules is in agreement with experimental,[34−37] simulation,[27−30,38] theoretical,[39] and self-consistent field calculation[40] results. Furthermore, for sufficiently long side chains, n_{sc} > 100, our model recovers a quadratic dependence of the Kuhn length on the bottlebrush diameter, $b_K \propto D^2/b$. For such long side the bottle-brush macromolecules are expected to behave as worm-like chains.[40−42]

Bottle-Brush Networks. In this section, we will discuss mechanical properties of bottle-brush networks obtained by random cross-linking of bottle-brush melts as described in Simulation Methods section. After cross-linking each bottle-brush molecule in a system with $k_{spring} = 30k_BT/\sigma^2$ has four cross-links, while systems with $k_{spring} = 500k_BT/\sigma^2$ have five cross-links per molecule randomly distributed along the bottle-brush backbone. The corresponding cross-linking densities are displayed in Table 1.

Stress−strain curves for uniaxially deformed networks are shown in Figure 10. The stress σ_{xx} generated in the network upon uniaxial deformation was obtained from the pressure tensor P_{ii} as follows:

DOI: 10.1021/acs.macromol.5b00682
Macromolecules 2015, 48, 5006−5015

Table 1. Parameters of Bottle-Brush Networks[a]

n_{sc}	K	G [k_BT/σ^3]	G_0 [k_BT/σ^3]	β_{fit}	β_{sim}	b_K/R_{max}	b_K/b	$\rho_{cr}\sigma^3$
			$k_{spring} = 30k_BT/\sigma^2$					
0	0.67	1.22×10^{-2}	1.32×10^{-2}	0.087	0.091	0.087	1.55	4.26×10^{-1}
5	2.04	2.28×10^{-3}	2.96×10^{-3}	0.213	0.167	0.17	3.38	7.26×10^{-2}
10	2.62	1.25×10^{-3}	1.76×10^{-3}	0.255	0.201	0.24	4.40	3.96×10^{-2}
15	3.10	9.28×10^{-4}	1.59×10^{-3}	0.350	0.233	0.31	5.28	2.59×10^{-2}
20	3.40	8.60×10^{-4}	1.46×10^{-3}	0.340	0.230	0.30	5.86	2.30×10^{-2}
			$k_{spring} = 500k_BT/\sigma^2$					
0	1.38	1.61×10^{-2}	1.89×10^{-2}	0.154	0.141	0.15	2.39	5.01×10^{-1}
2	2.09	6.50×10^{-3}	1.04×10^{-2}	0.337	0.190	0.22	3.46	1.69×10^{-1}
5	2.82	3.46×10^{-3}	5.78×10^{-3}	0.342	0.233	0.28	4.75	8.92×10^{-2}
7	3.30	2.49×10^{-3}	6.37×10^{-3}	0.501	0.258	0.35	5.67	6.49×10^{-2}
10	3.74	2.00×10^{-3}	6.16×10^{-3}	0.552	0.279	0.39	6.51	4.79×10^{-2}
12	4.03	1.50×10^{-3}	5.68×10^{-3}	0.605	0.295	0.43	7.09	4.01×10^{-2}
20	5.19	9.91×10^{-4}	4.74×10^{-3}	0.641	0.335	0.58	9.38	2.47×10^{-2}

[a] n_{sc} = number of monomers in side chains, K = bending constant of the bottlebrush obtained from eq 17; G = network shear modulus obtained from fitting $\sigma_{xx}(\lambda)$ curves in Figure 10 by using eq 15; G_0 = network shear modulus at small deformations, $\lambda \to 1$ (see eq 19); β_{fit} = value of the parameter β obtained from fitting $\sigma_{xx}(\lambda)$ curves in Figure 10 by using eq 15; β_{sim} = value of the parameter β obtained from simulations; ρ_{cr} = cross-linking density of bottle-brush networks; $R_{max} = bN_s$ = end-to-end distance of the fully extended bottle-brush backbone strand between cross-links; b_K = Kuhn length of bottle brush shown in Figure 4.

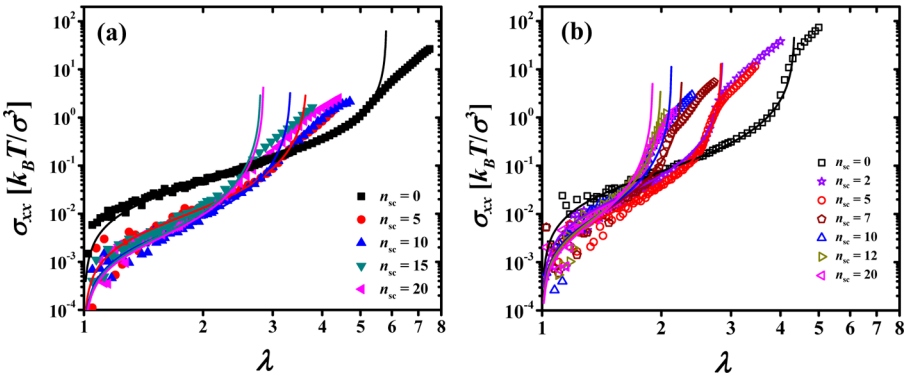

Figure 10. Dependence of the network stress σ_{xx} on the deformation (extension) ratio λ for bottle-brush networks obtained by cross-linking bottle-brush macromolecules with different side chain degree of polymerization, n_{sc}, and two different values of the FENE potential spring constants: (a) $k_{spring} = 30k_BT/\sigma^2$ and (b) $k_{spring} = 500k_BT/\sigma^2$.

$$\sigma_{xx} = \frac{3}{2}P_{xx} - \frac{1}{2}\sum_i P_{ii} \tag{14}$$

These data show that the bottle-brush networks are softer than the networks of linear chains. A transition to the nonlinear network deformation regime occurs earlier for bottle brushes with longer side chains as they have larger Kuhn length and backbone sections between cross-links are more stretched.

The lines in Figures 10a,b correspond to the best fit to the nonlinear network deformation model for which the true (physical) stress generated in the uniaxially deformed network is equal to[23]

$$\sigma_{xx}(\lambda) = \frac{G}{3}(\lambda^2 - \lambda^{-1}) \times \left(3 + \frac{2b_K}{b}\sqrt{K^2 + \left(1 - \frac{\beta I_1(\lambda)}{3}\right)^{-2}} - \frac{2b_K}{b}\sqrt{K^2 + 1}\right) \tag{15}$$

where $I_1(\lambda) = \lambda^2 + 2/\lambda$ is the first strain invariant of the deformation matrix for uniaxially deformed network with $\lambda_x = \lambda$; $\lambda_y = \lambda_z = 1/\sqrt{\lambda}$. The shear modulus of the network consisting of bottle-brush backbone strands can be written as

$$G \approx k_BT\frac{\tilde{\rho}}{N_s}\frac{\langle R_{in}^2\rangle}{b_K R_{max}} \approx k_BT\frac{\tilde{\rho}}{N_s}\frac{\beta R_{max}}{b_K} \tag{16}$$

where $\tilde{\rho}$ is the number density of backbone monomers that support the stress in the network, N_s is the number of backbone monomers between cross-links, and $\beta = \langle R_{in}^2\rangle/R_{max}^2$ is the ratio of the mean-square distance between cross-links in the undeformed network, $\langle R_{in}^2\rangle$, and the square of the end-to-end distance of the fully extended bottle-brush backbone strand, $R_{max} = N_s b$. Parameter β determines maximum possible extension of a backbone strand without bond deformation and varies between 0 and 1. Note that for flexible linear chains this parameter approaches zero while for fully extended backbone in densely grafted bottlebrushes with long side chains it is close to one. The value of the effective backbone bending constant K was obtained from bottlebrush Kuhn length, b_K, using the equation

$$b_K = b\frac{1 + \coth(K) - K^{-1}}{1 - \coth(K) + K^{-1}} \tag{17}$$

This mapping procedure allows us to describe a bottle brush by its backbone where effect of the side chains on the bottle-brush bending rigidity is absorbed into bending constant K. Note that

DOI: 10.1021/acs.macromol.5b00682
Macromolecules 2015, 48, 5006−5015

this representation is more convenient for comparison of properties of the bottle-brush networks and of those made of semiflexible chains. In our fitting procedure, we considered network shear modulus G and elongation ratio β as two fitting parameters. These values are summarized in Table 1. It follows from this table that the shear modulus G of the bottle-brush networks monotonically decreases with increasing the number of monomers in the side chains. This decrease occurs despite the increase of the value of the parameter β, which characterizes extension of network strands, and ascribed to two concurrent effect: (i) dilution of the network with side chains, n_{sc}, and (ii) stiffness increase of the network strands, b_K. Note that the deviation of analytical expression eq 15 from simulation data occurs in the interval of stresses where backbone bonds begin to deform. In this deformation regime, the network shear modulus is determined by the effective spring constant of the individual bonds. Also comparing values of the parameters β obtained from fitting of the stress−strain curves and those calculated from simulations, using end-to-end distance and number of monomers in the bottle-brush backbone between cross-links, we observe that difference between corresponding values of the parameter β increases with increasing ratio b_K/R_{max}. This indicates that for bottle-brush networks made of more rigid sections of the bottle-brush backbone between cross-links, the network elastic properties are determined by deformation of the shortest sections of the bottle-brush backbone that are closer to their fully extended conformations rather than the most representative ones.

It is useful to present eq 16 for the shear modulus in terms of the parameters describing the chemical structure of a bottlebrush network that include ρ − total monomer density in a system, N − number of monomers in the backbone, n_{cr} − number of cross-links per backbone, and n_{sc} − number of monomers in the side chains. Using these parameters, we can calculate the number of bottlebrushes per unit volume as $\rho/N(n_{sc} + 1)$. Each bottle brush in the system has $n_{cr} - 1$ backbone strands supporting stress in the network, each having in average N_s backbone monomers. Therefore, the density of the backbone monomers $\tilde{\rho}$ that participate in supporting stress is equal to $\tilde{\rho} = \rho(n_{cr} - 1)N_s/N(n_{sc} + 1)$. Using this expression for $\tilde{\rho}$, we can rewrite eq 16 as

$$G \propto k_B T \frac{\rho}{N} \frac{n_{cr} - 1}{n_{sc} + 1} \frac{\beta R_{max}}{b_K} \tag{18}$$

To verify eq 18, Figure 11 shows dependence of the reduced network modulus $G_{eff} = G[(n_{sc} + 1)/(n_{cr} - 1)]\beta^{-1}$ on the number of the Kuhn segments per strand R_{max}/b_K. In accordance with eq 18, the reduced shear modulus G_{eff} increases linear with increasing number of Kuhn segment per bottle-brush strands between cross-links.

In the linear network deformation regime, the value of the first strain invariant $I_1 \approx 3$. For such deformations, the shear modulus G_0 at small deformations is defined as follows:

$$G_0 \equiv \left.\frac{\sigma_{xx}(\lambda)}{\lambda^2 - \lambda^{-1}}\right|_{\lambda=1} = \frac{G}{3}\left(3 + \frac{2b_K}{b}\sqrt{K^2 + (1-\beta)^{-2}} - \frac{2b_K}{b}\sqrt{K^2 + 1}\right) \tag{19}$$

For networks with weakly extended strands ($\beta \approx b_K/R_{max} \ll 1$), eq 19 reduces to $G_0 \approx G$. The elastic response of these

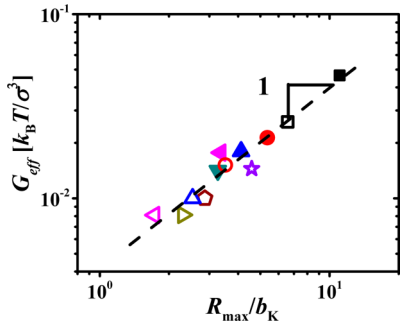

Figure 11. Dependence of the reduced network modulus $G_{eff} = G[(n_{sc} + 1)/(n_{cr} - 1)]\beta^{-1}$ on the number of Kuhn segments R_{max}/b_K per bottle-brush strand between cross-links for bottle-brush networks obtained by cross-linking bottle-brush macromolecules with different side chain degree of polymerization, n_{sc}, and two different values of the FENE potential spring constants, $k_{spring} = 30k_BT/\sigma^2$ and $k_{spring} = 500k_BT/\sigma^2$. Notations are the same as in Figure 10.

networks is controlled by entropic elasticity of the bottle-brush strands between cross-links. Figure 12a shows scaling dependence of $G_0/(n_{cr} - 1)$ on the side chain degree of polymerization. This representation allows us to collapse modulus data for systems with different number of cross-links per bottle brush. For short side chains our data can be described by a scaling law $G_0 \propto (n_{sc} + 1)^{-1}$. However, with increasing degree of polymerization of the side chains the simulation data deviate from the power law $G_0 \propto (n_{sc} + 1)^{-1}$, demonstrating a weaker dependence of the shear modulus G_0 on the degree of polymerization of the side chains. Note that this deviation correlates with a decrease in the number of the Kuhn segments per strand of the backbone between cross-links (see Table 1); i.e., bottlebrush stiffness increases with increasing a number of monomers in the side chains, n_{sc}. To illustrate this, in Figure 12b we show dependence of the ratio b_K/R_{max} on the parameter $K(1 - \beta)$, which controls crossover to semiflexible network deformation regime (see eq 19 and ref 23). In this range of parameters, the bottle-brush networks behave as networks of semiflexible chains. For such networks (see ref 23 for details) the strands between cross-links are almost fully stretched with $\beta \approx (1 - 2R_{max}/3b_K)$, and the shear modulus at small deformations, G_0, depends on the number of monomer in the side chains as

$$G_0 \approx \frac{2}{3}\frac{G}{(1-\beta)^2} \approx \frac{3}{2}k_BT\frac{\rho}{N}\frac{n_{cr} - 1}{n_{sc} + 1}\frac{b_K}{R_{max}} \propto n_{sc}^{-0.54} \tag{20}$$

In simplifying eq 20, we take into account that the Kuhn length of bottle brushes, b_K, scales with the degree of polymerization of the side chains as $b_K \propto n_{sc}^{0.46}$ (see Figure 4). Our simulation data, however, show slightly weaker dependence $G_0 \propto n_{sc}^{-0.5}$ than predicted by eq 20.

In the nonlinear network deformation regime, we can define the nonlinear network modulus

$$G(I_1) \equiv \frac{\sigma_{xx}(\lambda)}{\lambda^2 - \lambda^{-1}} \tag{21}$$

Analysis of the eq 15 for the network stress indicates that it is convenient to plot simulation data using reduced variables $G(I_1)/G$ as a function of $\beta I_1/3$. Figure 13 shows representation of our simulation data in these reduced variables. In the wide interval of network deformations our simulation data have

DOI: 10.1021/acs.macromol.5b00682
Macromolecules 2015, 48, 5006−5015

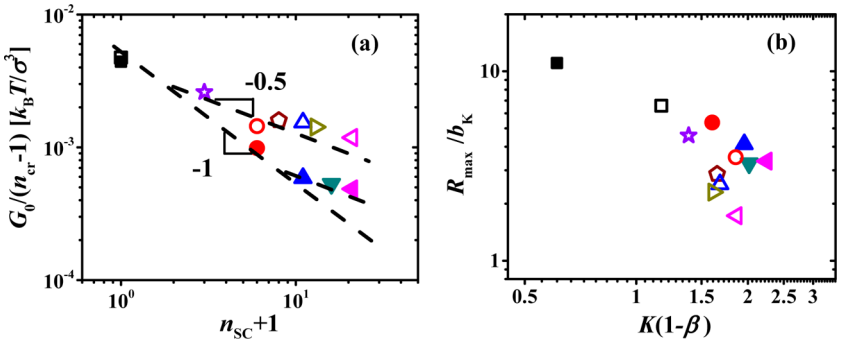

Figure 12. Dependence of the shear modulus on the side chain degree of polymerization (a) and of the number of Kuhn segments per bottle-brush backbone between cross-links R_{max}/b_K on the parameter $K(1-\beta)$ (b) for bottlebrush networks with two different values of the FENE potential spring constants: $k_{spring} = 30k_BT/\sigma^2$ and $k_{spring} = 500k_BT/\sigma^2$. Notations are the same as in Figure 10.

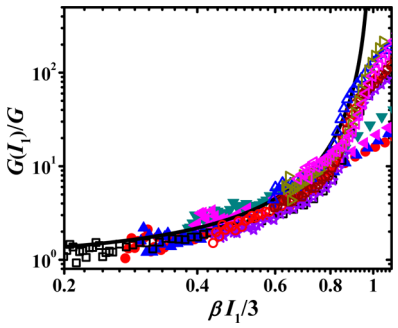

Figure 13. Dependence of the reduced network shear modulus $G(I_1)/G$ on the parameter $\beta I_1/3$ for bottle-brush networks. The solid line is given by eq 22. Notations are the same as in Figure 10.

collapsed, indicating universal behavior of the bottle-brush networks. It is important to point out that in the universal regime all our data can be described by a simplified version of the eq 15[22]

$$G(I_1) = \frac{G}{3}\left(1 + 2\left(1 - \frac{\beta I_1(\lambda)}{3}\right)^{-2}\right) \quad (22)$$

which is applicable to interval of the nonlinear network deformation where main contribution to the bottle-brush strand elasticity comes from bending modes. The deviation from universal behavior is observed in the range of the network deformations where the individual bonds of the bottle-brush backbone start to elongate.

Thus, theoretical analysis of the network deformations in linear and nonlinear deformation regimes indicates that the properties of the bottle-brush networks can be modeled by representing bottle-brush macromolecules as linear chains with an effective Kuhn length b_K and bending constant K.[23]

CONCLUSIONS

We study properties of the bottle-brush macromolecules in melts and in networks using molecular dynamics simulations and analytical calculations. Our analysis of the molecular dynamics simulations of the melt of bottle-brush macromolecules shows that the interactions between side chains makes bottle brushes stiffer (see Figure 4). The rigidity of the bottle-brush macromolecule monotonically increases with increasing degree of polymerization of the side chains as $b_K \propto n_{sc}^{0.46}$. However, the bottle-brush Kuhn segment is only slightly asymmetric with Kuhn length demonstrating almost linear dependence on the bottle-brush diameter, $b_K \propto D^{0.85}$. The bending rigidity of the bottle brush is entropic in nature and is due to redistribution of the side chains upon backbone bending (see Figure 8). Analysis of the simulation data indicates that the properties of bottle-brush macromolecules in a melt can be described by representing them as ideal chains with effective Kuhn length b_K.

This representation of the bottle-brush macromolecules can be extended to describe elastic properties of the bottle-brush networks in linear and nonlinear network deformation regime. The bottle-brush network shear modulus monotonically decreases with increasing side chain degree of polymerization (see Table 1). At small network deformations it scales with the degree of polymerization of the side chains, $G_0 \propto (n_{sc} + 1)^{-1}$, as shown in Figure 12a. The deviation from this scaling behavior takes place when the number of monomers in bottle-brush backbone between cross-links becomes on the order of number of monomers of the backbone within Kuhn length, b_K. These bottle-brush networks demonstrate behavior similar to those of networks of semiflexible chains. Shear modulus of such bottle-brush networks scales with the degree of polymerization of the side chains as $G_0 \propto n_{sc}^{-0.5}$. Thus, to take a maximum advantage of the effect of the side chains into the shear modulus of the bottlebrush networks, one should chose a cross-linking density in such a way to remain in the regime with $G_0 \propto (n_{sc} + 1)^{-1}$. In the nonlinear deformation regime the behavior of the bottle-brush networks is controlled by the bottle-brush bending modes (see Figure 13) and can be described in the frameworks of generalized network deformation model[23] based on discrete chain model with internal bending rigidity.[21]

SIMULATION METHODS

We have performed molecular dynamics simulations of melt of bottle-brush chains and deformation of bottle-brush networks. Each bottle-brush macromolecule consisted of a main chain backbone with the number of monomer $N = 100$ and side chains with the number of monomers n_{sc} attached to the every monomer of the backbone as shown in Figure 1. In our simulations we have varied the number of monomers in the side chains between 0 and 20 (see Table 2).

Bottle-brush chains were modeled by bead−spring chains made of beads with diameter σ. The nonbonded interactions between any two beads were described by the pure repulsive truncated-shifted Lennard-Jones (LJ) potential[20]

DOI: 10.1021/acs.macromol.5b00682
Macromolecules 2015, 48, 5006−5015

Table 2. Studied Systems

n_{sc}	number of beads	$L_x = L_y = L_z$ [σ]
0	10000	23.0
2	30000	33.5
5	60000	42.2
7	80000	46.4
10	110000	51.6
12	130000	54.6
15	160000	58.5
20	210000	64.0

$$U_{LJ}(r_{ij}) = \begin{cases} 4\varepsilon_{LJ}\left[\left(\frac{\sigma}{r_{ij}}\right)^{12} - \left(\frac{\sigma}{r_{ij}}\right)^{6} - \left(\frac{\sigma}{r_{cut}}\right)^{12} + \left(\frac{\sigma}{r_{cut}}\right)^{6}\right] & r_{ij} \le r_{cut} \\ 0 & r_{ij} > r_{cut} \end{cases} \quad (23)$$

where r_{ij} is the distance between the ith and jth beads and σ is the bead (monomer) diameter. The cutoff distance for the bead−bead interactions was set to $r_{cut} = 2^{1/6}\sigma$, and the value of the Lennard-Jones interaction parameter ε_{LJ} was equal to $1.5k_BT$ (where k_B is the Boltzmann constant and T is the absolute temperature). The connectivity of the beads into bottle-brush chains was maintained by the finite extension nonlinear elastic (FENE) potential

$$U_{FENE}(r) = -\frac{1}{2}k_{spring}R_{max}^{2}\ln\left(1 - \frac{r^2}{R_{max}^{2}}\right) \quad (24)$$

with the values of the spring constant $k_{spring} = 500k_BT/\sigma^2$ and $30k_BT/\sigma^2$ and the maximum bond length $R_{max} = 1.5\sigma$. The large value of the spring constant was selected to minimize the effect of the bond stretching at large network deformations. The repulsive part of the bond potential was modeled by the truncated-shifted Lennard-Jones (LJ) potential with the value of LJ interaction parameter $\varepsilon_{LJ} = 1.5k_BT$ and $r_{cut} = 2^{1/6}\sigma$. The average bond length $\langle b^2\rangle^{1/2} = 0.837\sigma$ for $k_{spring} = 500k_BT/\sigma^2$ and 0.987σ for $k_{spring} = 30k_BT/\sigma^2$.

Simulations were carried out in a constant number of particles and temperature ensemble. The constant temperature was maintained by coupling the system to a Langevin thermostat implemented in LAMMPS.[43] In this case, the equation of motion of the ith bead is

$$m\frac{d\vec{v}_i(t)}{dt} = \vec{F}_i(t) - \xi\vec{v}_i(t) + \vec{F}_i^{R}(t) \quad (25)$$

where m is the bead mass set to unity for all beads in a system, $\vec{v}_i(t)$ is the bead velocity, and $\vec{F}_i(t)$ is the net deterministic force acting on the ith bead. The stochastic force $\vec{F}_i^{R}(t)$ had a zero average value and δ-functional correlations $\langle\vec{F}_i^{R}(t)\cdot\vec{F}_i^{R}(t')\rangle = 6k_BT\xi(t - t')$. The friction coefficient ξ coupling a system to a Langevin thermostat was set to $\xi = 0.1m/\tau_{LJ}$, where τ_{LJ} is the standard LJ time, $\tau_{LJ} = \sigma(m/\varepsilon_{LJ})^{1/2}$. The velocity-Verlet algorithm with a time step $\Delta t = 0.005\tau_{LJ}$ was used for integration of the equations of motion. In our simulations we used 3-D periodic boundary conditions. All simulations were performed using LAMMPS.[43]

First we have prepared melt of bottle-brush macromolecules. The system was initialized by placing 100 bottle-brush chains in a simulation box with monomer concentration equal to $0.1\sigma^{-3}$. Then the system was compressed until the monomer density reached $0.8\sigma^{-3}$. The final box dimensions are listed in Table 2.

After completion of the compression step the system was equilibrated for 10^8 integration steps. Note that the required duration of the simulation runs was established by monitoring relaxation of the autocorrelation function of the bottlebrush backbone $\langle\vec{R}_e(t)\vec{R}_e(t + \Delta t)\rangle$. To obtain bottle-brush network, the monomers belonging to the bottle-brush backbone were randomly cross-linked. This was done by randomly selecting pairs of monomers that fall within 5.0σ distance from each other. One cross-link bond was allowed per bottle-brush backbone monomer. The final average number of cross-links per bottle-brush backbone was equal to 5.0 for $k_{spring} = 500k_BT/\sigma^2$ and 4.0 for $k_{spring} = 30k_BT/\sigma^2$. The other network parameters are summarized in Table 3.

Table 3. Bottle-Brush Network Parameters

n_{sc}	no. of cross-links per chain	av no. of monomers between cross-links[a] $\langle N_s\rangle$	cross-linking density $\rho_{cr}\sigma^3$
		$k_{spring} = 30k_BT/\sigma^2$	
0	4.0	17.7	1.60×10^{-2}
5		18.1	2.67×10^{-3}
10		18.1	1.45×10^{-3}
15		17.2	1.00×10^{-3}
20		19.6	0.76×10^{-3}
		$k_{spring} = 500k_BT/\sigma^2$	
0	5.0	15.7	2.00×10^{-2}
2		15.8	6.67×10^{-3}
5		16.7	3.33×10^{-3}
7		16.2	2.50×10^{-3}
10		16.5	1.82×10^{-3}
12		16.3	1.54×10^{-3}
20		16.2	0.95×10^{-3}

[a]In calculating average number of monomers between cross-links, we have excluded dangling ends' contribution.

In order to relax the networks, the cross-link bond potential was initially modeled by a harmonic potential with a spring constant $K_h = 10k_BT/\sigma^2$. For the network with $k_{spring} = 500k_BT/\sigma^2$, the cross-link spring constant K_h was gradually increased with an increment of $\Delta K_h = 30k_BT/\sigma^2$ until it has reached $500k_BT/\sigma^2$. For the network with $k_{spring} = 30k_BT/\sigma^2$, the cross-link spring constant K_h was increased with an increment of $\Delta K_h = 10k_BT/\sigma^2$ until it has reached $30k_BT/\sigma^2$. The duration of each step during which the spring constant was incrementally increased was 2×10^5 integration steps. After that the potential was replaced by FENE potential with the same parameters as one used to model bonds of the bottle-brush chains. Networks were equilibrated by performing NVT molecular dynamics simulation runs lasting 10^8 integration steps.

In order to obtain stress−strain relation for bottle-brush networks, we have performed sets of simulation runs of uniaxial network deformations.[44−46] This deformation was achieved by a series of small affine deformation steps $\{x_i, y_i, z_i\} \rightarrow \{\Delta\lambda x_i, y_i/(\Delta\lambda)^{1/2}, z_i/(\Delta\lambda)^{1/2}\}$ with an increment $\Delta\lambda = 0.025$. This incremental deformation was achieved by performing simulations of network deformation at constant deformation rate lasting 5×10^5 integrations steps. After this step the network was equilibrated for 2×10^6 integrations steps, which was followed by a production run lasting 3×10^6 integration steps.

AUTHOR INFORMATION

Corresponding Author

*E-mail avd@ims.uconn.edu (A.V.D.).

DOI: 10.1021/acs.macromol.5b00682
Macromolecules 2015, 48, 5006−5015

Notes

The authors declare no competing financial interest.

■ ACKNOWLEDGMENTS

The authors are grateful to the National Science Foundation for the financial support under Grants DMR-1409710, DMR-1407645, and DMR-1436201. This work was performed at the U.S. Department of Energy, Center for Integrated Nanotechnologies, at Los Alamos National Laboratory (Contract DE-AC52-06NA25396) and Sandia National Laboratories. Sandia is a multiprogram laboratory operated by Sandia Corporation, a Lockheed Martin Company, for the United States Department of Energy under Contract DE-AC04-94AL85000. J.-M.Y.C's contribution was sponsored by the Office of Advanced Scientific Computing Research, U.S. Department of Energy, and performed at the Oak Ridge National Laboratory, which is managed by UT-Battelle, LLC, under Contract De-AC05-00OR22725.

■ REFERENCES

(1) Treloar, L. R. G. *The Physics of Rubber Elasticity*; Oxford University Press: Oxford, UK, 1975.
(2) Rubinstein, M.; Colby, R. *Polymers Physics*; Oxford University Press: Oxford, UK, 2003.
(3) Doi, M.; Edwards, S. F. *The Theory of Polymer Dynamics*; Clarendon Press: Oxford, UK, 1986.
(4) Langer, R.; Tirrell, D. A. *Nature* **2004**, *428*, 487−492.
(5) Discher, D. E.; Janmey, P. A.; Wang, Y. L. *Science* **2005**, *310*, 1139−1143.
(6) Williams, D. F. *Biomaterials* **2008**, *29*, 2941−2953.
(7) Urayama, K.; Kawamura, T.; Kohjiya, S. *J. Chem. Phys.* **1996**, *105*, 4833−4840.
(8) Urayama, K.; Kawamura, T.; Kohjiya, S. *Polymer* **2009**, *50*, 347−356.
(9) Inkson, N. J.; Graham, R. S.; McLeish, T. C. B.; Groves, D. J.; Fernyhough, C. M. *Macromolecules* **2006**, *39*, 4217−4227.
(10) Kapnistos, M.; Vlassopoulos, D.; Roovers, J.; Leal, L. G. *Macromolecules* **2005**, *38*, 7852−7862.
(11) Pakula, T.; Vlassopoulos, D.; Fytas, G.; Roovers, J. *Macromolecules* **1998**, *31*, 8931−8940.
(12) Milner, S. T.; McLeish, T. C. B. *Macromolecules* **1998**, *31*, 7479−7482.
(13) Likos, C. N.; Löwen, H.; Watzlawek, M.; Abbas, B.; Jucknischke, O.; Allgaier, J.; Richter, D. *Phys. Rev. Lett.* **1998**, *80*, 4450−4453.
(14) Grayson, S. M.; Frechet, J. M. *Chem. Rev.* **2001**, *101*, 3819−3868.
(15) Zeng, F.; Zimmerman, S. C. *Chem. Rev.* **1997**, *97*, 1681−1712.
(16) Neugebauer, D.; Zhang, Y.; Pakula, T.; Sheiko, S. S.; Matyjaszewski, K. *Macromolecules* **2003**, *36*, 6746−6755.
(17) Pakula, T.; Zhang, Y.; Matyjaszewski, K.; Lee, H.-i.; Boerner, H.; Qin, S.; Berry, G. C. *Polymer* **2006**, *47*, 7198−7206.
(18) Zhang, Y.; Costantini, N.; Mierzwa, M.; Pakula, T.; Neugebauer, D.; Matyjaszewski, K. *Polymer* **2004**, *45*, 6333−6339.
(19) Hu, M.; Xia, Y.; McKenna, G. B.; Kornfield, J. A.; Grubbs, R. H. *Macromolecules* **2011**, *44*, 6935−6943.
(20) Frenkel, D.; Smit, B. *Understanding Molecular Simulations: From Algorithms to Applications*; Academic Press: New York, 2002.
(21) Dobrynin, A. V.; Carrillo, J.-M. Y.; Rubinstein, M. *Macromolecules* **2010**, *43*, 9181−9190.
(22) Dobrynin, A. V.; Carrillo, J.-M. Y. *Macromolecules* **2011**, *44*, 140−146.
(23) Carrillo, J.-M. Y.; MacKintosh, F. C.; Dobrynin, A. V. *Macromolecules* **2013**, *46*, 3679−3692.
(24) Gubarev, A.; Carrillo, J.-M. Y.; Dobrynin, A. V. *Macromolecules* **2009**, *42*, 5851−5860.
(25) Carrillo, J.-M. Y.; Dobrynin, A. V. *Macromolecules* **2010**, *43*, 2589−2604.
(26) Carrillo, J.-M. Y.; Dobrynin, A. V. *Macromolecules* **2011**, *44*, 5798−5816.
(27) Saariaho, M.; Ikkala, O.; Szleifer, I.; Erukhimovich, I.; tenBrinke, G. *J. Chem. Phys.* **1997**, *107*, 3267−3276.
(28) Saariaho, M.; Szleifer, I.; Ikkala, O.; ten Brinke, G. *Macromol. Theory Simul.* **1998**, *7*, 211−216.
(29) Hsu, H. P.; Paul, W.; Binder, K. *Macromolecules* **2010**, *43*, 3094−3102.
(30) Hsu, H. P.; Paul, W.; Binder, K. *Macromol. Theory Simul.* **2011**, *20*, 510−525.
(31) Hsu, H.-P.; Paul, W.; Binder, K. *Europhys. Lett.* **2010**, *92*, 28003−1−6.
(32) Grosberg, A. Y.; Khokhlov, A. R. *Statistical Physics of Macromolecules*; AIP Press: New York, 1994.
(33) Knight, K. *Mathematical Statistics*; Chapman and Hall: New York, 1999.
(34) Rathgeber, S.; Pakula, T.; Wilk, A.; Matyjaszewski, K.; Lee, H.-i.; Beers, K. L. *Polymer* **2006**, *47*, 7318−7327.
(35) Lecommandoux, S.; Chécot, F.; Borsali, R.; Schappacher, M.; Deffieux, A.; Brûlet, A.; Cotton, J. P. *Macromolecules* **2002**, *35*, 8878−8881.
(36) Feuz, L.; Strunz, P.; Geue, T.; Textor, M.; Borisov, O. *Eur. Phys. J. E: Soft Matter Biol. Phys.* **2007**, *23*, 237−245.
(37) Zhang, Z.; Carrillo, J.-M. Y.; Ahn, S.-k.; Wu, B.; Hong, K.; Smith, G. S.; Do, C. *Macromolecules* **2014**, *47*, 5808−5814.
(38) Theodorakis, P. E.; Hsu, H.-P.; Paul, W.; Binder, K. *J. Chem. Phys.* **2011**, *135*, 164903.
(39) Birnstein, T. M.; Borisov, O. V.; Zhulina, Y. B.; Khokhlov, A. R.; Yurasova, T. A. *Polym. Sci. U.S.S.R.* **1987**, *29*, 1293−1300.
(40) Feuz, L.; Leermakers, F. A. M.; Textor, M.; Borisov, O. *Macromolecules* **2005**, *38*, 8891−8901.
(41) Fredrickson, G. H. *Macromolecules* **1993**, *26*, 2825−2831.
(42) Subbotin, A.; Saariaho, M.; Ikkala, O.; ten Brinke, G. *Macromolecules* **2000**, *33*, 3447−3452.
(43) Plimpton, S. J. *J. Comput. Phys.* **1995**, *117*, 1−19.
(44) Svaneborg, C.; Everaers, R.; Grest, G. S.; Curro, J. G. *Macromolecules* **2008**, *41*, 4920−4928.
(45) Svaneborg, C.; Grest, G. S.; Everaers, R. *Phys. Rev. Lett.* **2004**, *93*, 257801.
(46) Svaneborg, C.; Grest, G. S.; Everaers, R. *Polymer* **2005**, *46*, 4283−4295.

DOI: 10.1021/acs.macromol.5b00682
Macromolecules 2015, 48, 5006−5015